JPG Journal of Petroleum Geology www.jpg.co.uk

Journal of Petroleum Geology, Vol. 40(2), April 2017, pp 173-193

HYDROCARBON GENERATION POTENTIAL AND DEPOSITIONAL ENVIRONMENT OF SHALES IN THE CRETACEOUS NAPO FORMATION, EASTERN ORIENTE BASIN, ECUADOR

Xiao-Fa Yang *+, Yin-Fu Xie*, Zhi-Wei Zhang*, Zhong-Zhen Ma*, Yu-Bing Zhou*, Ya-Ming Liu*, Dan-Dan Wang*, and Yong-Bin Zhao*

Marine shale samples from the Cretaceous (Albian-Campanian) Napo Formation (n = 26) from six wells in the eastern Oriente Basin of Ecuador were analysed to evaluate their organic geochemical characteristics and petroleum generation potential. Geochemical analyses included measurements of total organic carbon (TOC) content, Rock-Eval pyrolysis, pyrolysis – gas chromatography (Py–GC), gas chromatography – mass-spectrometry (GC–MS), biomarker distributions and kerogen analysis by optical microscopy. Hydrocarbon accumulations in the eastern Oriente Basin are attributable to a single petroleum system, and oil and gas generated by Upper Cretaceous source rocks is trapped in reservoirs ranging in age from Early Cretaceous to Eocene.

The shale samples analysed for this study came from the upper part of the Napo Formation T member ("Upper T"), the overlying B limestone, and the lower part of the U member ("Lower U"). The samples are rich in amorphous organic matter with TOC contents in the range 0.71–5.97 wt% and Rock-Eval T_{max} values of 427–446°C. Kerogen in the B Limestone shales is oil-prone Type II with $\delta^{13}C$ of -27.19 to -27.45‰; whereas the Upper T and Lower U member samples contain Type II–III kerogen mixed with Type III ($\delta^{13}C$ > -26.30‰). The hydrocarbon yield (S_2) ranges from 0.68 to 40.92 mg HC/g rock (average: 12.61 mg HC/g rock). Hydrogen index (HI) values are 427–693 mg HC/g TOC for the B limestone samples, and 68–448 mg HC/g TOC for the Lower U and Upper T samples.

The mean vitrinite reflectance is 0.56–0.79% R_o for the B limestone samples and 0.40–0.60% R_o for the Lower U and Upper T samples, indicating early to mid oil window maturity for the former and immature to early maturity for the latter. Microscopy shows that the shales studied contain abundant organic matter which is mainly amorphous or alginite of marine origin.

Extracts of shale samples from the B limestone are characterized by low to medium molecular weight compounds (n-C_{14} to n-C_{20}) and have a low Pr/Ph ratio (≈ 1.0), high phytane/n-C_{18} ratio (1.01–1.29), and dominant C_{27} regular steranes. These biomarker

* PetroChina Research Institute of Petroleum Exploration & Development, Beijing 100083, China.
+ corresponding author, email: ouyangxiaofa@petrochina.com.cn

Key words: marine shales, source rock, Cretaceous, Napo Formation, Oriente Basin, Ecuador, hydrocarbon potential.

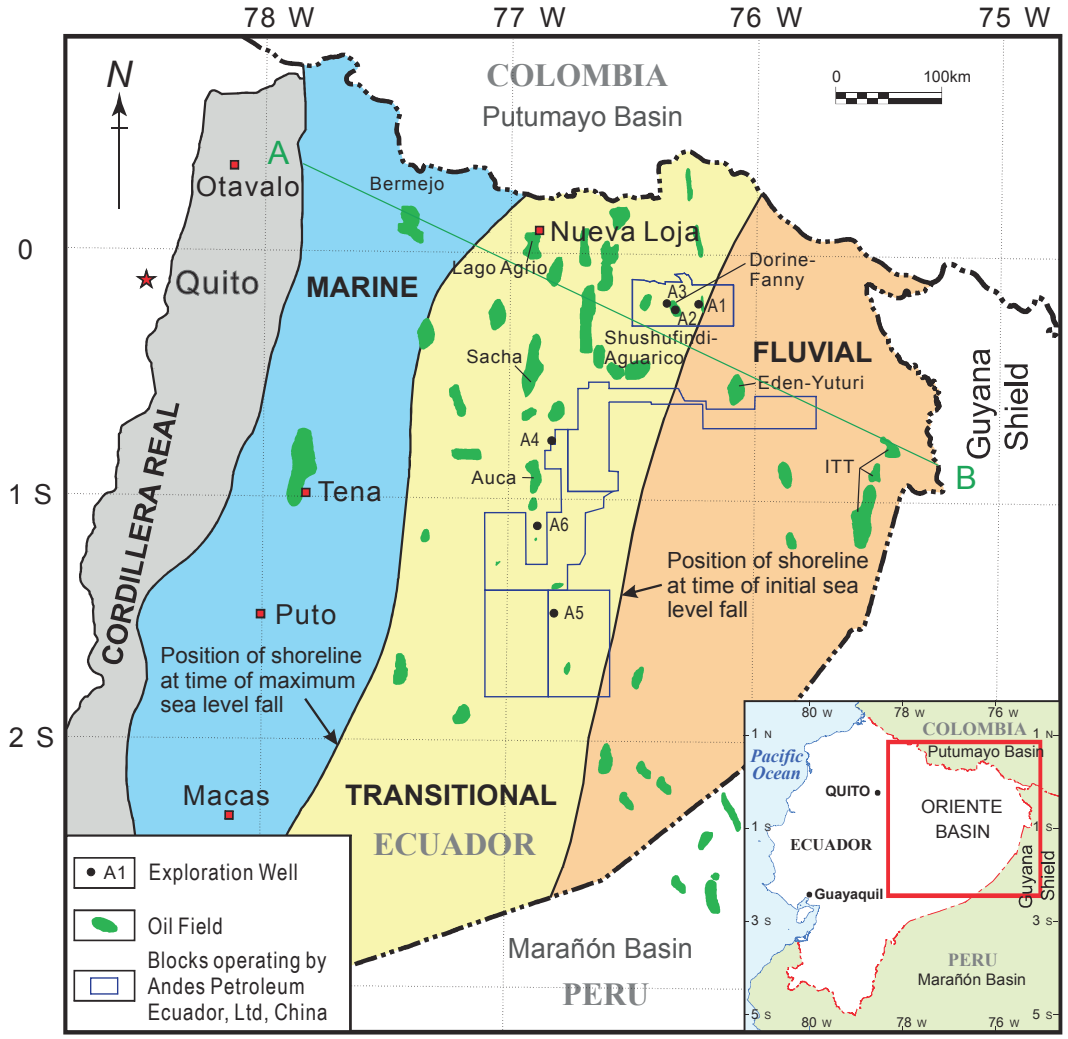

Fig. 1. Simplified structure map of the Oriente Basin in Ecuador with the location of wells A1-A6 from which shales were sampled (adapted from Baby *et al.*, 2013; Estupiñan *et al.*, 2010; White *et al.*, 1995). Colours indicate Napo Formation palaeogeography. The yellow (transitional) area is bounded to the east by the position of coastline at the time of initial sea level fall during Napo Formation deposition, and to the west by the position of the coastline during maximum seal-level fall.

parameters and the abundant amorphous organic matter indicate that the organic matter was derived from marine algal material and was deposited under anoxic conditions. By contrast, the extracts from the Lower U and Upper T shales contain medium to high molecular weight compounds (n-C_{25} to n-C_{31}) and have a high Pr/Ph ratio (>3.0), low phytane/n-C_{18} ratio (0.45–0.80) with dominant C_{29} regular steranes, consistent with an origin from terrigenous higher plant material mixed with marine algae deposited under suboxic conditions. This is also indicated by the presence of mixed amorphous and structured organic matter.

This new geochemical data suggests that the analysed shales from the Napo Formation, especially the shales from the B limestone which contain Type II kerogen, have significant hydrocarbon potential in the eastern part of the Oriente Basin. The data may help to explain the distribution of hydrocarbon reserves in the east of the Oriente Basin, and also assist with the prediction of non-structural traps.

INTRODUCTION

Most of Ecuador's oil reserves are located in the Oriente Basin (Fig. 1), part of the Marañón – Oriente – Putumayo foreland system (Marksteiner and Aleman, 1997) which extends from Peru in the south to Colombia in the north (Higley, 2001; Mathalone and Montoya, 2005). The Oriente Basin covers an area of nearly 100,000 km^2 and is one of the most prolific of the sub-Andean basins (Baby *et al.*, 2013; Canfield *et al.*, 1985; Dashwood and Abbotts, 1990; Tschopp, 1953) with reserves of approximate 34.5 billion barrels (brl) of oil and cumulative oil production of 4.8 billion brl (IHS database, 2015). The basin has attracted the interest of numerous researchers and oil companies, and its stratigraphy, tectonics, petroleum geochemistry and petroleum geology have been the subject of detailed investigation (Baby *et al.*, 2013; Brookfield *et al.*, 2009; Dashwood and Abbotts, 1990; Estupiñan *et al.*, 2007, 2010; Feininger, 1975; Hu *et*

al., 2010; Jaillard, 1997; Jaillard *et al*.,, 2005; Pindell and Tabbutt, 1995; Shanmugam *et al*., 2000; Smith, 1989; White *et al*., 1995; Xie *et al*., 2010).

Organic-rich marine claystones and fine-grained limestones in the Albian-Campanian Napo Formation are considered to be major source rocks for hydrocarbons in the Oriente Basin (Dashwood and Abbotts, 1990; Gaibor *et al*., 2008; Pindell and Tabbutt, 1995; Tschopp, 1953; Vallejo *et al*., 2002; White *et al*., 1995). The formation also contains major sandstone reservoir units, and a regional seal is provided by the overlying Paleocene red beds. However, in spite of the long history of oil exploration and production (Feininger, 1975; Tschopp, 1953), few studies of source rocks in the eastern part of the basin have been published (Baby *et al*., 2013; Dashwood and Abbotts, 1990; Feininger, 1975). Moreover, the source rock quality and maturity of the Napo shales, and the distance of oil migration in the eastern Oriente Basin, are still debated (Baby *et al*., 2013; Dashwood and Abbotts, 1990; Feininger, 1975). Thus some authors have proposed that the Napo Formation is generally immature in the east/north of the Oriente Basin, and that hydrocarbons have migrated from mature source kitchens located in the western part of the basin, or in northern Peru or southern Columbia (Canfield *et al*., 1985; Dashwood and Abbotts, 1990; Feininger, 1975).

For this paper, Napo Formation shale samples were collected from six exploration wells in the eastern Oriente Basin (wells A1-A6: Fig. 1), and were analysed in terms of petrography, biomarker distributions, thermal maturity and hydrocarbon generating potential, and their depositional setting was interpreted.

GEOLOGICAL SETTING

The sub-Andean foreland basin system is located to the east of the Andes Mountains and extends for over 6400 km from Venezuela to Argentina. The Oriente Basin in Ecuador is part of the foreland zone between the Andean Cordilleras to the west and the Guayana or Brazilian shield to the east (Dashwood and Abbotts, 1990; Tschopp, 1953) (Fig. 1). The Mesozoic geological evolution of this area was largely controlled by a change in the geometry of subduction of the oceanic Nazca plate beneath the western margin of northern South America; this geometry evolves from flat-slab subduction in Peru to more oblique subduction in Colombia (Gutscher *et al*., 1999).

Structurally, the Oriente Basin is characterized by the presence of overprinted structures (Balkwill *et al*., 1995; Barragán *et al*., 2005). Pre-Cretaceous extensional systems, inherited from NNE–SSW Triassic and Jurassic rifts (Christophoul *et al*., 2002), have been tectonically inverted along a NNE–SSW dextral strike-slip transpressive system, which has deformed the foreland basin system since the Late Cretaceous (Baby *et al*., 2013).

The Oriente Basin is bounded to the west by the Sub-Andean "foot-hills" fold-and-thrust belt at the eastern margin of the Cordillera Real (Fig. 1), which comprises the Napo uplift in the north and the Cutucú uplift in the south (Baby *et al*., 2013; Christophoul *et al*., 2002). These uplifts consist of large-scale fold structures bounded by thrust faults. To the east of the foldbelt, the forebulge-backbulge portion of the Oriente Basin is weakly deformed by NNE–SSW trending *en échelon* reverse faults, which controlled the development of structures at major oil fields (Baby *et al*., 2013).

Some 148 oil fields are located within the Oriente Basin, of which 95 are currently in production with total output of more than 510,000 brl per day. The main phase of development drilling occurred in the late 1970s and early 1980s. Among the largest oilfields in the east of the basin are Shushufindi-Aguarico, Sacha and Auca (Fig. 1) with reserves of 3.85, 3.45, 1.32 billion brl, respectively. Hydrocarbon accumulations in the basin are attributable to a single petroleum system. Oil and gas have been generated by Upper Cretaceous source rocks in the Napo Formation, and are trapped in reservoir sandstones which range in age from Early Cretaceous to Eocene (Higley, 2001). Peak hydrocarbon generation probably took place during the Oligocene (Canfield *et al*., 1985). No hydrocarbon production has been reported from reservoirs of Palaeozoic age (Higley, 2001). Geologic and geochemical data suggests that hydrocarbons were generated from Lower Cretaceous source rocks located in the NW part of the Marañón Basin and the deeper southern part of the Oriente Basin (Baby *et al*., 2013).

Stratigraphy

The Precambrian cratonic basement of the Oriente Basin consists mostly of igneous and metamorphic rocks (Feininger, 1975; Tschopp, 1953), and is overlain by a sedimentary cover ranging in age from Late Silurian to Cenozoic. The cover can be divided by regional unconformities into pre-Cretaceous, Cretaceous, and post-Cretaceous (molasse) successions (Fig. 2) (Baby *et al*., 2013; Dashwood and Abbotts, 1990).

The pre-Cretaceous interval ranges in age from Late Silurian to Jurassic (Fig. 2) and is divided into four formations (Dashwood and Abbotts, 1990). The Pumbuiza Formation (Upper Silurian – Lower Devonian) comprises deformed and mildly metamorphosed limestones, slates, slaty shales and sandstones. These are overlain by up to 750 m of thinly-bedded carbonates and shales of the Macuma Formation which represent the deposits of an extensive, Pennsylvanian to Early Permian shallow-marine

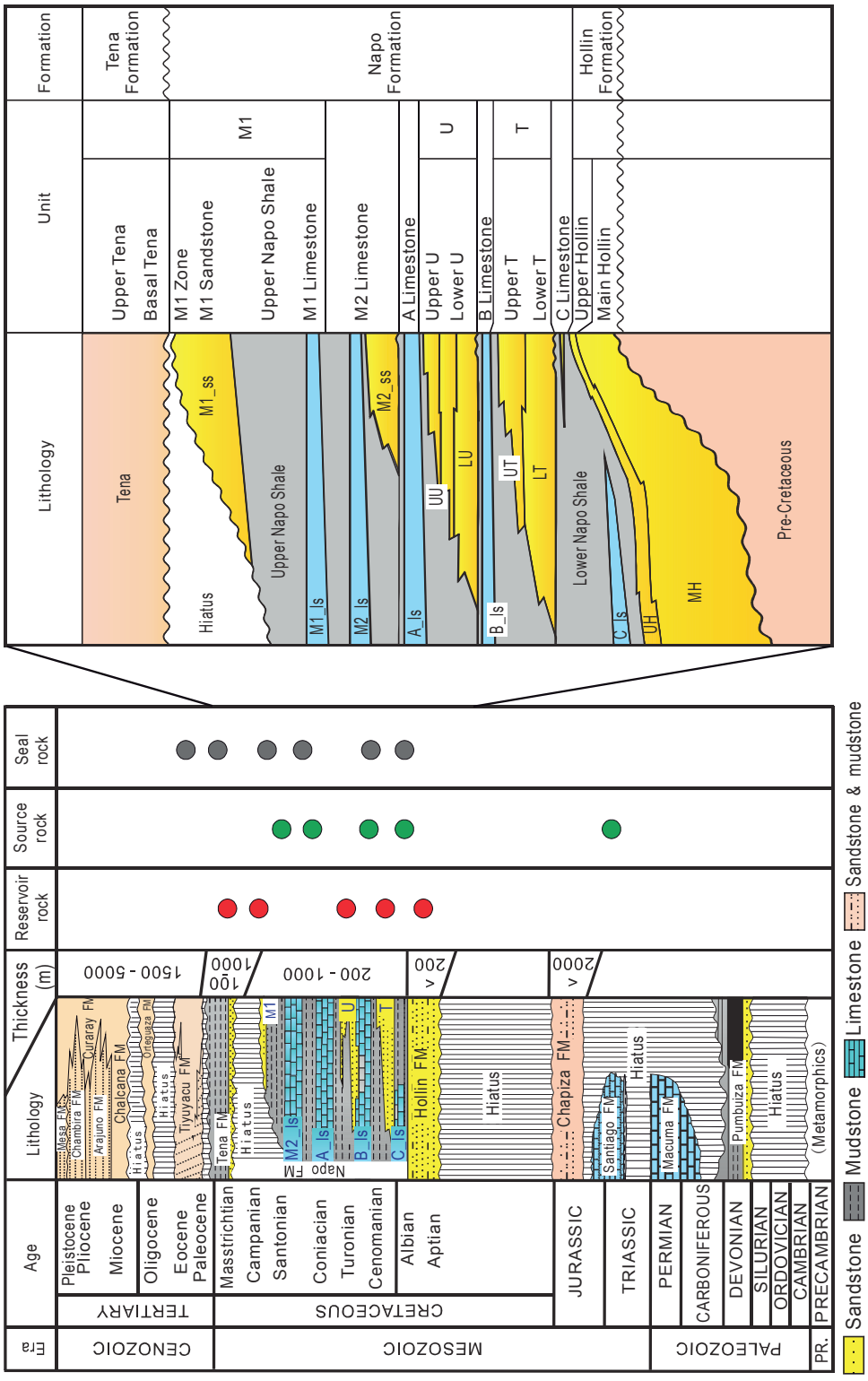

Fig. 2. Generalised stratigraphic column for the Oriente Basin with lithostratigraphic nomenclature (modified after Dashwood and Abbotts, 1990).

carbonate shelf. The overlying Santiago Formation is composed of grey to black limestones, calcareous sandstones and organic-rich shales deposited in intracratonic rift basins during the Norian – Toarcian (Gaibor *et al.*, 2008; Tschopp, 1953). Finally the Chapiza Formation consists of grey to red siltstones, sandstones, conglomerates and volcanics deposited in a back-arc extensional basin (Pindell and Tabbutt, 1995).

The Cretaceous succession was deposited following a major depositional hiatus (about 120–110 Ma) (Jaillard, 1997) and can be divided into the basal Hollin Formation, the Napo Formation and the Tena Formation (Dashwood and Abbotts, 1990) (Fig. 2). The Hollin Formation consists of widespread sandstones deposited in braided fluvial and littoral environments during a rapid marine transgression.

The conformably overlying Napo Formation consists of a sequence of marine claystones, limestones and sandstones whose maximum thickness exceeds 700m. The formation comprises a succession of easterly-sourced, fluvial and deltaic/estuarine deposits which prograded westwards into shoreline and marine shelf settings (Dashwood and Abbotts, 1990; Shanmugam *et al*., 2000; White *et al*., 1995) (Fig. 1).

The Napo Formation is informally divided into seven members (Higley, 2001) (Fig. 2): the C limestone, the T sandstone, the B limestone, the U sandstone, the A limestone, and the M2 and M1 sandstones. The Napo U and T have been subdivided into upper and lower parts (Upper and Lower U, and Upper and Lower T). The lower parts of these units consist mainly of quartzose sandstones, while the upper parts are composed of glauconitic sandstones interbedded with burrowed mudstones and fossiliferous wackestones containing abundant calcareous nannofossils, and occasional planktonics and other bioclasts (White *et al*., 1995; Yang *et al*., 2016b). The shales were deposited on a stable marine shelf during transgressive periods (Dashwood and Abbotts, 1990). OM-rich intervals in the claystones and carbonate mudstones appear to be the main source rocks in the basin, while the Napo T, U, M2 and M1 sandstones are significant oil reservoirs (Canfield *et al*., 1985; Dashwood and Abbotts, 1990; Higley, 2001; Shanmugam *et al*., 2000; White *et al*., 1995; Yang *et al*., 2016a) (Fig. 2).

The Tena Formation conformably overlies the Napo Formation in the eastern part of the basin but is progressively truncated westwards. The overlying Cenozoic molasse succession is 4000-5000 m thick in the south of the basin and less than 1500 m thick in the north (Dashwood and Abbotts, 1990). The fluvial-dominated Tiyuyacu Formation (Eocene) unconformably overlies the Tena Formation (Christophoul *et al*., 2002; Tschopp, 1953), and is overlain by the Orteguaza (Upper Eocene to Oligocene) which comprises up to 300 m of fluvial and marine claystones (Canfield *et al*., 1985; Christophoul *et al*., 2002). The basin fill is completed by up to 3000 m of Miocene to Recent continental red beds of the diachronous Chalcana, Arajuno, Chambira and Mesa Formations (Dashwood and Abbotts, 1990) (Fig. 2).

SAMPLING AND METHODS

Sampling

The top and bottom surfaces of the Napo Formation are in general relatively easy to identify and correlate in the Oriente Basin using core, well-log and seismic data (Estupiñan *et al*., 2010; White *et al*., 1995). In particular, the Napo Upper T glauconitic sandstones can be traced throughout the whole Oriente Basin, and are even present at outcrops in the western foothills (Yang *et al*., 2016b). Therefore, the Napo U, T and B limestone can be correlated reliably in the eastern Oriente Basin.

Twenty-six shale core samples from the Napo Formation were collected from six exploration wells (A1-A6, Fig. 1) in the eastern Oriente Basin. Shale samples were recovered from the Napo Formation Lower U, B limestone and Upper T members over a depth interval of 8140 – 12,345 ft (2481-3763m) (Table 1). The shale samples underwent geochemical analyses including TOC measurements, Rock-Eval pyrolysis, and extraction followed by GC (gas chromatography) and GC–MS (gas chromatography mass-spectrometry) of saturated hydrocarbons.

Petrographic and mineralogical analyses

Microscope studies used a Nikon ECLIPSE LV 100 POL instrument, and SEM analyses used a FEI Quanta 200F equipped with an energy dispersive spectrometer (EDS). Kerogen observation was carried out under ultraviolet light using a fluorescence microscope Zeiss Axio Zmager AI. The vitrinite reflectance (%R_o) of kerogen macerals was measured on selected samples using an MPV3 microphotometer with a 50× oil immersion objective under reflected white light.

Organic geochemistry

The 26 samples were analysed for TOC using a LECOTM Carbon-Sulfur 230 analyzer and were pyrolysed using a Rock-Eval II unit (Espitalié *et al*., 1977). Parameters measured included S_1, the volatile hydrocarbon content, in mg HC/g rock; S_2, the remaining hydrocarbon generative potential, mg HC/g rock; and the temperature of maximum pyrolysis yield (T_{max}, °C). Values of the Hydrogen Index (HI) were calculated (Espitalié *et al*., 1977) and in combination with T_{max} were used to determine the kerogen type (Tissot and Welte, 1984).

Contents of carbon, hydrogen, oxygen and nitrogen were determined using a Vario EL Cube Analyzer by Elementar. The $\delta^{13}C$ values of the kerogen were measured using a Finngan MAT-252 apparatus with an ambient temperature of 25 °C and humidity of 20%.

Fourteen shale samples were selected for more detailed source rocks analyses and were Soxhlet-extracted with chloroform for approximately 72h. Asphaltenes in the shale extracts were removed by *n*-hexane precipitation. The deasphaltened shale extracts were then separated into saturated and aromatic hydrocarbon fractions by silica gel and alumina column chromatography.

GC analysis of the saturated hydrocarbon fraction was conducted on a SHIMADZU GC-2010 chromatograph equipped with an HP-5 fused silica column (30m×0.25mm×0.25μm). The oven temperature was initially set at 100 °C for 1 min,

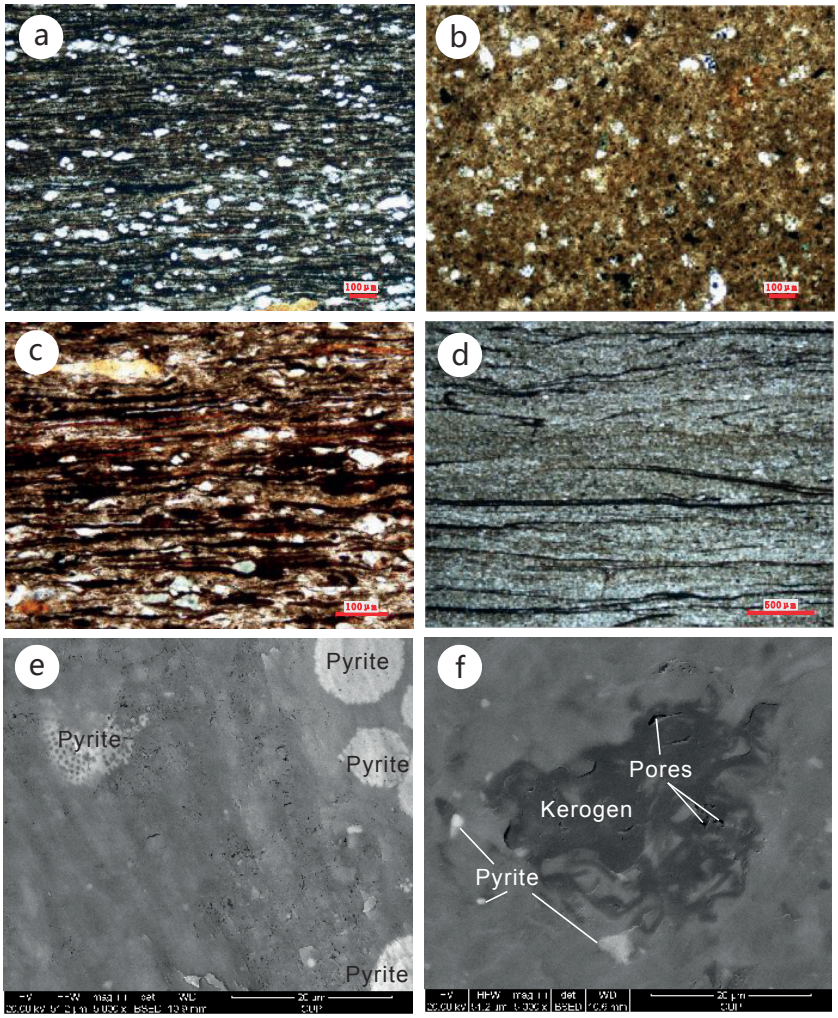

Fig. 3. Photomicrographs (a-d) of typical laminated organic-rich shales (plane-polarized light): (a) calcareous shale, sample M-13 from the Napo B limestone; elongate wisps of organic material are oriented parallel to the lamination; depth 10,380ft, well A2. (b) calcareous shale, sample M-11 from the B limestone with abundant planktonic foraminifera and scattered organic material together with local glauconite; depth 10,378ft, well A2. (c) clay-dominated shale with thin, lenticular silt alternating with argillaceous and organic material parallel to the lamination; sample M-02 from the Upper T shale, depth 8139ft; well A1. (d) clay-dominated shale with thin, lenticular silt alternating with argillaceous and organic material which lies parallel to the lamination; sample M-17 from the Lower U shale, depth 9356ft, well A3. SEM images (e-f) of organic-rich shales show pyrite, kerogen and pores: (e) carbonate-rich argillaceous shale, sample M-11 from the B limestone, depth 10,378 ft, well A2; and (f) argillaceous shale, sample M-17 from the Lower U shale, depth 9356ft in well A2.

and programmed to 300 °C at 4 °C /min with a final hold at 300 °C for 25 min. Helium was utilized as the carrier gas.

GC–MS was carried out on the saturated and aromatic fractions using an Agilent 6890GC/5975iMS instrument equipped with an HP-5MS capillary column (60m × 0.25mm × 0.25μm). The temperature programme for saturated hydrocarbons was 50 °C for 1 min, 50–120 °C at 20 °C/min, 120–310 °C at 3 °C/min, and finally held for 25 min at 310 °C. The temperature programme for aromatic hydrocarbons was 80 °C for 1 min, 80–310 °C at 3 °C/min, and a final hold for 25 min at 310 °C. The temperature of the injector was 300 °C. Helium was used as the carrier gas at a flow rate of 1 ml/min. The scan range was from 50–550 Da using full scan and selected ion monitoring (SCAN/SIM) modes at 70 eV. Biomarker ratios were calculated from peak areas of individual compounds.

The analytical work took place at the State Key Laboratory of Petroleum Resources and Prospecting, and the Department of Organic Geochemistry and Environmental Science, China University of Petroleum (Beijing).

RESULTS AND DISCUSSION

Petrography and mineralogy

The Napo B limestone member consists of interbedded grey-black carbonate-rich shales and grey limestones. The shales are calcareous, locally pyritic, slightly silty to very finely sandy. Elongate discontinuous organic wisps are oriented parallel to bedding (Fig. 3a).

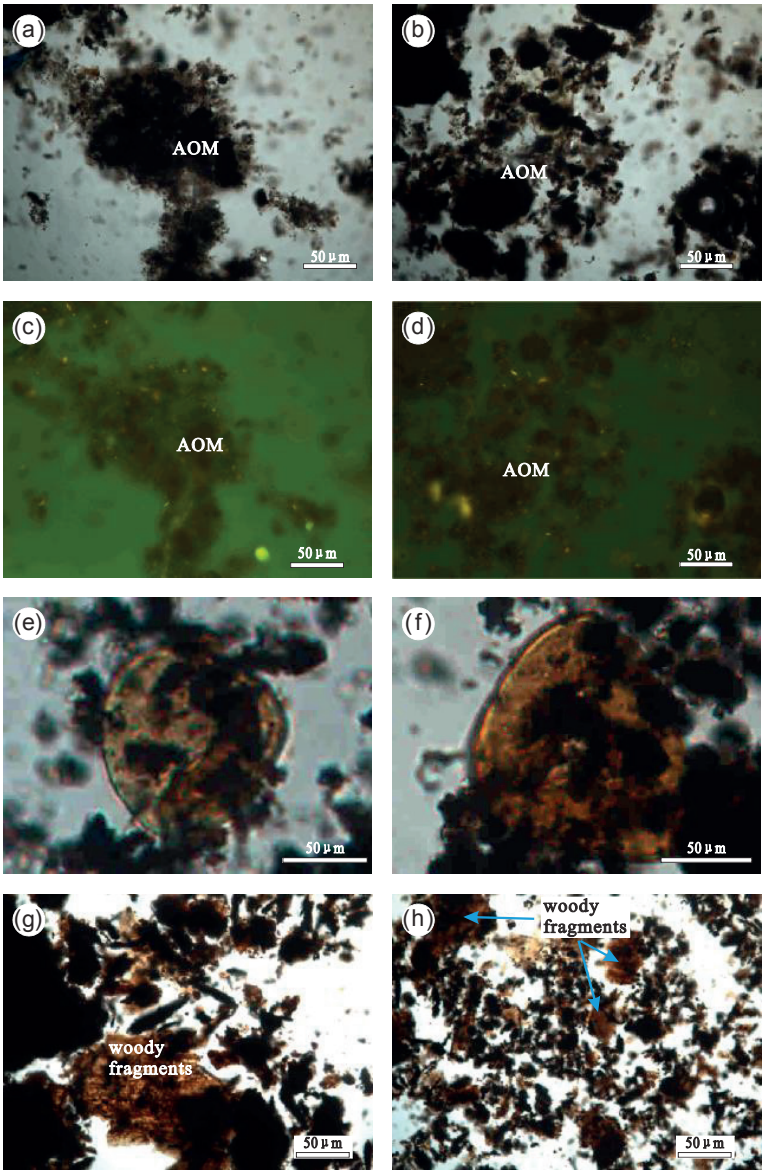

Fig. 4. Photomicrographs of kerogen in the Cretaceous Napo shales under transmitted and plane-polarized incident fluorescence. (a-b) Amorphous organic matter (white transmitted light): (a) calcareous shale, sample M-10 from the B limestone, depth 10,369ft, well A2; (b) carbonate-rich argillaceous shale, sample M-12 from the B limestone, depth 10,379ft, well A2.
(c, d) as (a) and (b) but under UV light, showing amorphous organic matter.
(e, f) structured organic matter (spores and pollen) in (e) argillaceous shale, sample M-17 from the Lower U shale, depth 9356ft, well A3 (white transmitted light); and (f) argillaceous shale, sample M-12 from the B limestone, depth 10,379ft in well A2.
(g, h) phytoclasts in: (g) clay-dominated shale, sample M-14 in well A2, Upper T, shale 10,422ft; and (h) carbonate-rich argillaceous shale, sample M-03, Upper T shale, depth 8139ft, well A1.

The principal silt-sized components of the shale are quartz. XRD data indicate that the total clay fraction of the calcareous shales is about 36% to 57.5% by weight (Table 3). Mixed-layer illite/smectite are the predominant clay minerals (Yang *et al*., 2016a). The Napo B limestone shales also include massive, highly fossiliferous dark greyish to black shales which contain abundant calcareous microfossils (planktonic foraminifera) as observed in thin section (Fig. 3b).

The Upper T shales are very dark to black claystones, which have rhythmic bedding of sandstone lenses. In thin section, the Upper T shales are characterised by thin, lenticular silt intervals alternating with argillaceous and organic material. The principal silt-sized components are quartz with minor K-feldspar. In thin section, elongate, discontinuous organic materials oriented parallel to bedding form dark brown lamellae (Fig. 3c). Diagenetic minerals present include abundant pyrite (Fig. 3e). XRD data indicate that the total clay fraction of these shales is 44% to 85% by weight (Table 3).

The Lower U shales are composed of dark grey to black, laminated claystones with irregular lenses of bioturbated sandy material (Fig. 3d), and some

Table 1. Bulk geochemical results of Rock–Eval / TOC analysis with calculated parameters, vitrinite reflectance (%R_o) and $\delta^{13}C$ of the Napo shale samples. B_ls = B limestone, UT = Upper T, LU = Lower U.

Member	Well	Sample	Measured Depth (ft)	TOC (%)	Rock–Eval pyrolysis						Kerogen			
					S1 (mg/g)	S2 (mg/g)	Tmax (°C)	HI (mg/g)	P I		H/C	O/C	R_o (%)	δ^{13}CPDB(‰)
B_ls	A1	M-01	8104	2.92	1.31	16.27	436	557	0.07		1.35	0.05	0.71	-27.2
	A2	M-08	10366	1.65	0.64	7.04	437	427	0.08					
		M-09	10368	2.12	0.87	11.61	439	548	0.07					
		M-10	10369	1.61	0.70	7.54	438	468	0.08		1.17	0.06	0.79	-27.3
		M-11	10378	2.79	1.43	19.25	442	690	0.07					
		M-12	10379	3.27	1.66	21.53	439	658	0.07		1.40	0.05	nd	-27.3
		M-13	10380	3.14	1.81	21.75	438	693	0.08		1.23	0.05	0.56	-27.5
UT	A1	M-02	8139	5.82	1.28	23.75	440	408	0.05					
		M-03	8140	5.97	1.83	26.76	438	448	0.06		1.12	0.09	0.40	-24.6
		M-05	8161	4.26	1.38	16.12	438	378	0.08		1.01	0.10	0.47	-24.8
		M-06	8163	4.23	1.09	16.04	436	379	0.06					
		M-07	8165	4.20	1.52	17.84	438	425	0.08		1.12	0.10	0.49	-24.9
	A2	M-14	10422	4.57	1.49	17.20	441	376	0.08		1.17	0.12	0.50	-25.0
	A4	M-20	10234	1.50	0.31	3.59	442	239	0.08		1.06	0.07	0.45	-25.8
		M-21	10261	1.61	0.48	4.25	441	264	0.10					
		M-22	10286	1.73	0.62	4.68	440	271	0.12					
	A5	M-23	12191	0.71	0.07	0.68	438	95	0.09		1.08	0.09	0.45	-27.4
		M-24	12324	1.62	0.21	1.76	441	109	0.11					
	A6	M-25	12326	1.23	0.10	1.99	438	162	0.05		1.07	0.12	0.45	-25.9
		M-26	12345	1.84	0.61	3.88	435	211	0.14					
		M-27	10366	5.23	0.37	3.56	440	68	0.09		0.97	0.09	0.45	-24.3
		M-28	10375	3.66	0.83	7.85	437	214	0.10					
LU	A3	M-16	9284	3.28	1.54	11.56	434	352	0.12					
		M-17	9356	4.15	0.87	12.64	439	305	0.06		1.02	0.12	0.60	-26.3
		M-18	9361	3.08	0.54	7.91	446	257	0.06					
		M-19	9374	5.89	3.13	40.92	427	695	0.07		1.52	0.25	0.47	-21.5

TOC, total organic carbon, wt%; S_1, volatile hydrocarbon (HC) content, mg HC/g rock; S_2, remaining HC generative potential, mg HC/g rock; T_{max}, temperature at S_2 peak; PY, potential yield = $S_1 + S_2$ (mg/g); HI, hydrogen index = $S_2 \times 100$/TOC mg HC/g TOC; PI, production index = $S_1/(S_1 + S_2)$.

small scattered patches of organic material. Macerated plant fragments are common together with amorphous organic material. Pyrite is dispersed throughout the clay matrix (Fig. 3f).

Microscope examination showed that the shales have some brown staining due to bitumen (Fig. 3a and b). Pyrite was present (Fig. 3c) and, in association with organic matter, indicated that the shales were deposited under anoxic conditions. Palynofacies identified in the samples comprise structured organic matter (SOM) and amorphous organic matter (AOM) (Fig. 4). Microporosity was observed in aggregates of AOM (Fig. 3f). The AOM is dominated by brightly fluorescent amorphous bituminite (Figs. 3 and 4) which is finely disseminated and degraded and is interpreted to include altered algal material, microbial biomass, solid bitumen and some live oil (c.f. Hackley and SanFilipo, 2016; Hutton *et al*., 1994).

AOM was dominant (43–85%, average 69%) in the kerogen assemblage of the shale samples, with abundant SOM (i.e. phytoclasts) in some samples (Fig. 4e and f). The AOM appears to be aggregated and granular (Fig. 4a-d) and was brown-dark coloured under white light (Fig. 4b). Yellow-brown fluorescence intensities were observed under ultraviolet light (Fig. 4c and d). Fluorescent AOM is of marine origin (Tissot and Welte, 1984).

Mineral composition by wt% from XRD analyses of the Napo shale samples are presented in Table 2 which shows that clays, quartz, pyrite, feldspar, calcite and siderite were present. There is in general a dominance of clay minerals (Table 2) mixed with quartz, pyrite and other minerals.

The B limestone shales have higher carbonate content than the Lower U and Upper T shales. The lithology of the B limestone shales is dominated by calcareous mudstones, while the Lower U and Upper T shales are argillaceous mudstones or claystones.

Source rock characteristics

The Napo shale samples have a TOC content of 0.71–5.97% (Table 1), with Rock-Eval S_2 of >2.0 mg HC/g rock (Table 1), indicating that they have very good to excellent source rock potential (Fig. 5). The samples analysed have HI values of 68–695 mg HC/g TOC (Table 1) and T_{max} of 434–446 °C. Mean vitrinite reflectance (VR) for the shale samples ranges between 0.5% and 0.7% R_o (Table 1), indicating that they have early to peak oil window maturity.

A cross-plot of hydrogen index (HI) versus pyrolysis T_{max} can be used to classify the type of organic matter and the thermal maturity (Mukhopadhyay *et al*., 1995) (Fig. 6). In general, the Napo shale samples plot in the early mature to mature zone of Type II, II–III and III kerogens. The B limestone samples plot within the Type II field, whereas the Lower U and Upper T samples plot in the Type II–III field grading to Type III. A graph of atomic H/C versus O/C ratios (Fig. 7) also indicates that most samples contain Types II and II–III kerogen.

Table 2. Mineral composition of the Napo shale samples on the basis of quantitative X-ray diffraction (XRD) analysis. B_ls = B limestone, UT = Upper T, LU = Lower U.

Member	Well	Samples	Minerals							
			Quartz (wt%)	K-Fdsp (wt%)	Plag. (wt%)	Calcite (wt%)	Siderite (wt%)	Pyrite (wt%)	Barite (wt%)	Clay (wt%)
B_ls	A1	M-01	20.7	2.0	-	35.5	1.9	4.0	-	36.0
	A2	M-08	25.7	-	-	11.8	4.5	3.9	-	54.2
		M-10	26.9	-	-	12.3		3.2	-	57.5
		M-11	26.9	-	-	19.0	1.9	2.9	-	49.3
		M-13	23.6	-	-	17.1	1.2	3.2	-	54.9
UT	A1	M-03	23.1	4.0	-	-	-	5.5	-	67.4
		M-07	12.7	-	-	-	-	1.9	-	85.4
	A2	M-14	16.0	-	-	-	-	7.9	-	76.1
	A4	M-20	31.6	4.2	-	-	-	2.2	-	62.1
	A5	M-23	26.4	3.1	-	2.9	-	3.9	-	63.7
	A6	M-25	38.2	8.3	5.5	-	-	-	-	48.0
		M-27	33.1	-	-	-	23.1	-	-	43.8
LU	A3	M-17	25.9	-	-	-	-	17.8	-	56.3
		M-19	10.2	-	-	21.2	-	14.0	2.9	51.7

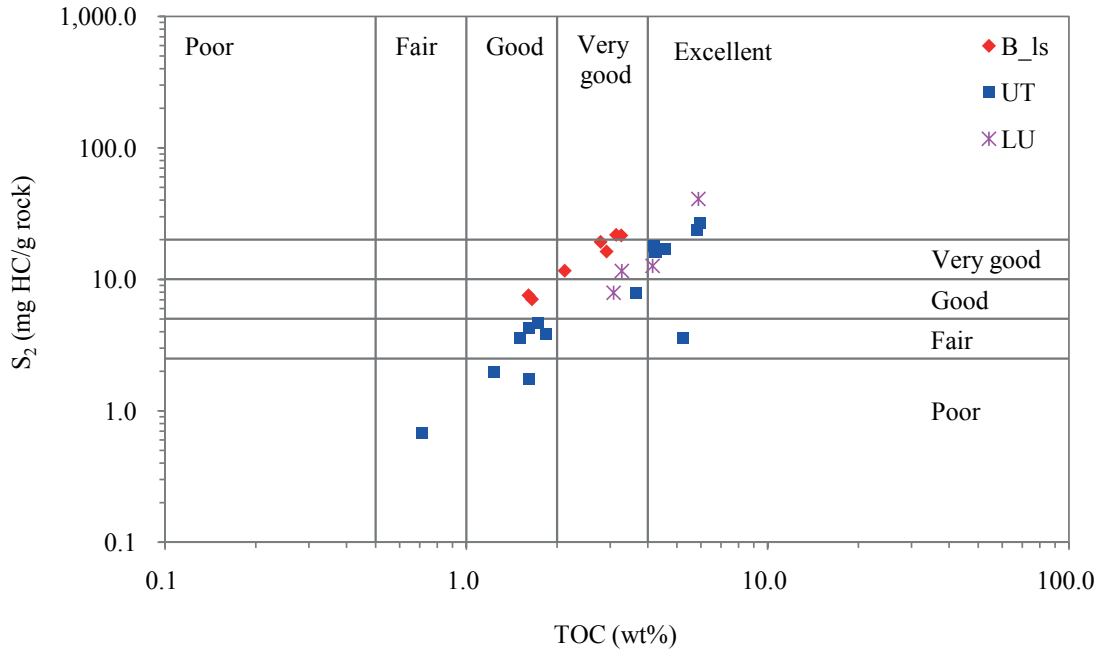

Fig. 5. Cross-plot of pyrolysis S_2 versus total organic carbon (TOC) for the Napo Formation shales from wells in the study area showing the generative source rock potential. B_ls = B limestone, UT = Upper T, LU = Lower U.

Kerogen type can also been classified in terms of $\delta^{13}C$ values (Huang *et al*., 1984). The $\delta^{13}C$ of kerogen in shales from the B limestone samples ranges from –27.19 to –27.45‰, whereas the $\delta^{13}C$ values of kerogen from the Upper T and Lower U shale samples is > -26.30‰ (Table 1). This suggests that the kerogen in the B limestone samples is Type II, but that the Upper T and Lower U samples mainly contain Type II–III kerogen with minor Type III.

The Rock–Eval pyrolysis data and kerogen $\delta^{13}C$ are consistent with the kerogen type observed under the microscope which was dominated by amorphous organic matter (Fig. 4).

Thermal maturity

The thermal maturity of organic matter in the Napo shales was evaluated based on vitrinite reflectance (%R_o), pyrolysis T_{max} data, and biomarker maturity parameters (Peters *et al*., 2005). The B limestone shale samples (with Type II OM) had mean VR of 0.56–0.79% R_o, and the LU and UT shale samples (with Type II–III and III kerogen) had mean VR of about 0.40–0.60% R_o (Table 1). Thermogenic oil is thought to be generated at vitrinite reflectance values above 0.6% for Types I and II kerogen (Bordenave, 1993), and the VR data therefore suggests that the B limestone shales are sufficiently mature to generate oil.

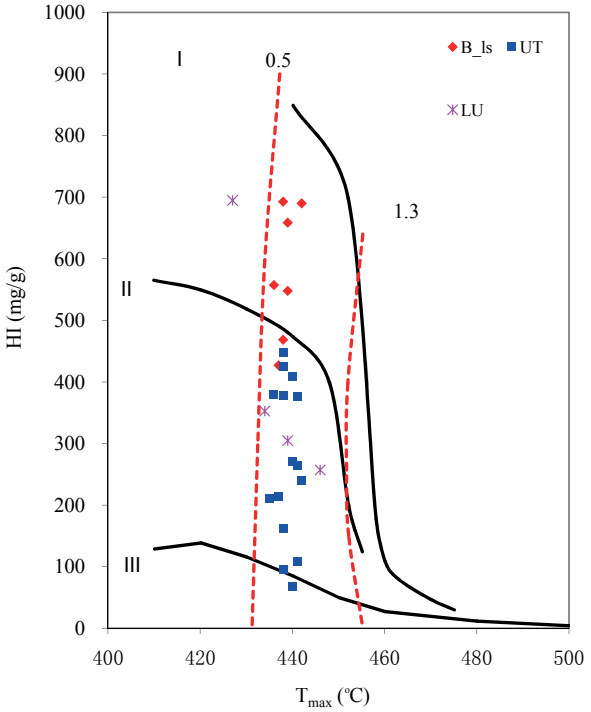

Fig. 6. Cross-plot of hydrogen index (HI) versus pyrolysis T_{max} for the analysed Napo shale samples, showing kerogen quality and thermal maturation. The graph shows that the shale samples show similar pyrolysis T_{max} values and that in general two types of kerogen are present. B_ls = B limestone, UT = Upper T, LU = Lower U.

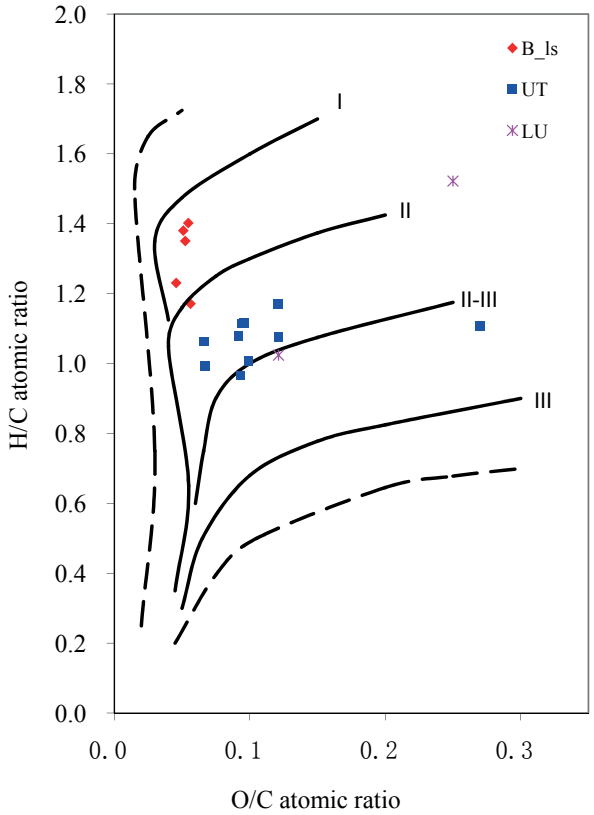

Fig. 7. Cross-plot of atomic H/C versus O/C ratios for the shale samples from the Napo Formation. B_ls = B limestone, UT = Upper T, LU = Lower U. In contrast to the Rock-Eval data (Fig. 6), the cross-plot shows that the B limestone shales contain Type II kerogen, while the Lower U and Upper T shales contain predominantly kerogen Type II-III.

The thermal maturity of organic matter in the analysed samples was also evaluated from the Rock-Eval T_{max} peak, which varies for different types of OM (Bordenave, 1993; Peters, 1986; Tissot and Welte, 1984); the peak is relatively narrow for Type I kerogen, wider for Type II and much wider for Type III kerogen due to the increasing structural complexity of the organic matter (Tissot *et al*., 1987). This is consistent with the composition of the analysed B limestone shale samples which contain peak-mature Type II kerogen, and the Lower U and Upper T samples which contain immature or early mature Type II–III and Type III kerogen (Figs 6 and 7).

Values of the Carbon Preference Index (CPI), calculated using the formula $2(C_{23} + C_{25} + C_{27} + C_{29})/[C_{22} + 2(C_{24} + C_{26} + C_{28}) + C_{30}]$ (Peters *et al*., 2005),

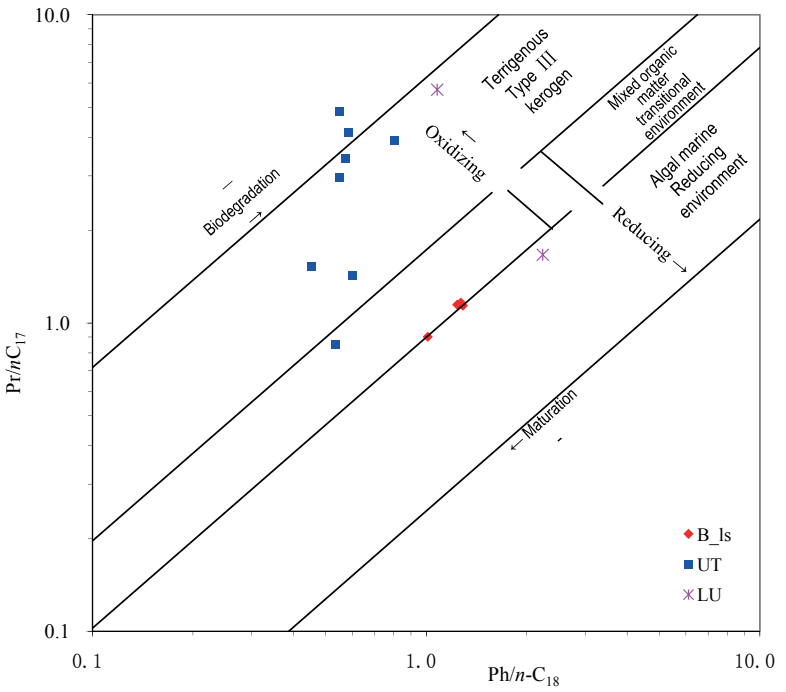

Fig. 8. Cross-plot of pristane / n-C_{17} versus phytane / n-C_{18} (after Shanmugam, 1985) which is used to infer the oxicity and organic matter type in the source-rock depositional environment. The cross-plot shows that the B limestone shales contain algal marine OM deposited in anoxic conditions, while the Upper T and Lower U shales contain terrigenous organic matter deposited under suboxic conditions. B_ls = B limestone, UT = Upper T, LU = Lower U.

range from 1.04 to 1.13 indicating that the extracted shale samples from the B limestone are thermally mature. CPI values for the Lower U and Upper T shale extracts are relatively high (1.11-1.47) (Table 3). The relationship between Pr/n-C_{17} and Ph/n-C_{18} ratios (Fig. 8) is consistent with this interpretation.

Biomarker parameters such as C_{32} 22S/(22S + 22R) homohopane, moretane/hopane and 20S/(20S + 20R), and ββ/(ββ + αα) C_{29} sterane ratios were also used as maturity indicators (Mackenzie *et al*., 1980; Waples and Machihara, 1991). The C_{32} homohopanes 22S/(22S + 22R) ratio for the shale extracts is 0.53–0.59 (Table 3), suggesting that they have reached equilibrium values in the oil window. The 20S/(20S + 20R) and ββ/(ββ + αα) regular C_{29} sterane ratios range from 0.31 – 0.47 and 0.30–0.40, respectively (Table 3), which indicates early to mature oil window range (Waples and Machihara, 1991). The moretane/hopane ratios are consistent with low relative abundance of C_{30} moretane (Fig. 9b, e and h). The extracts from the B limestone shales have moretane/hopane ratios of 0.22–0.25, suggesting the samples are early to peak mature (Waples and Machihara, 1991) (Fig. 10). The biomarker maturation parameters are consistent with the observed vitrinite reflectance data.

Oil generation potential

Organic geochemical data and petrographic results indicate that the Napo shales have very good petroleum generation potential. Most of the shales from the B limestone have a relatively high hydrogen index (HI) ranging from 427 to 693 mg HC/g TOC, indicating predominantly Type II kerogen (Fig. 6) derived from marine algal organic matter which mainly consists of fluorescing amorphous organic matter (Figs 4c and d). The Type II–III and III kerogen with HI values between 68 and 448 mg HC/g TOC is oil and gas prone.

The production index (PI) is calculated according to the formula Rock-Eval $S_1/(S_1+S_2)$. High PI values are usually interpreted to be due to migrated hydrocarbons (Hasenhüttl *et al*., 2001), but the index will be underestimated if the expulsion saturation threshold is low (Law, 1999). Expulsion of hydrocarbons probably leads to lower PI values. The PI values from the B limestone shale samples are 0.07-0.08, and the PI values from Upper T and Lower U shale samples vary from 0.05 to 0.14 (Table 1). The relationship between PI and T_{max} indicates that the B limestone shale samples are thermally mature and that hydrocarbons have already been generated (Fig. 12).

Organic matter input and depositional environment

Source input and depositional setting were interpreted using biomarker data including distributions of normal alkanes and isoprenoids, steranes (*m/z* 217) and triterpanes (*m/z* 191).

Normal alkanes and isoprenoids

Gas chromatograms of saturated hydrocarbon fractions from extracts of the Napo Shale samples are shown in Fig. 9 and derived parameters are listed in Table 3. The gas chromatograms display a full suite of n-alkanes between $C_{13}$and C_{34}. Three types of n -alkane distribution were distinguished. Firstly (Fig. 9a), there was a unimodal distribution with a predominance of low to medium molecular weight compounds (n-C_{14} to n-C_{20}) with an absence of odd-over-even carbon number

Table 3. *n*-Alkane and isoprenoids ratios and biomarker parameters of selected Napo shale samples dependent on source and maturity.

Member	Well	Sample	n-Alkanes and isoprenoids					Triterpanes and terpanes (m/z 191)						Steranes and diasteranes (m/z 217)						
			Pr/Ph	Pr/C_{17}	Ph/C_{18}	CPI	OEP	C_{32} 22S/ (22S+22R)	C_{29}/ C_{30}	Ts/ Tm	MC30/ HC30	H index	G/ C_{30}	C_{29} 20S/ (20S+20R)	C_{29} ββ/ (ββ+αα)	C_{29}/ C_{27}	Regular steranes (%)			Diasteranes/ steranes
																	C_{27}	C_{28}	C_{29}	
B_ls	A1	M-01	1.13	1.15	1.24	1.08	1.05	0.56	0.27	0.61	0.22	0.09	0.25	0.31	0.32	0.65	0.42	0.3	0.27	0.94
	A2	M-10	1.07	0.90	1.01	1.13	1.07	0.57	0.31	0.65	0.25	0.09	0.26	0.37	0.40	0.64	0.43	0.3	0.27	1.21
		M-12	1.07	1.14	1.29	1.06	0.98	0.58	0.26	0.75	0.24	0.09	0.39	0.37	0.37	0.59	0.44	0.3	0.26	1.22
		M-13	1.08	1.16	1.27	1.04	0.99	0.56	0.26	0.92	0.24	0.09	0.42	0.35	0.36	0.59	0.44	0.3	0.26	1.13
UT	A1	M-03	10.52	4.84	0.55	1.33	1.34	0.57	0.74	0.12	0.30	0.03	0.11	0.42	0.31	2.76	0.19	0.3	0.53	0.51
		M-05	4.67	3.92	0.80	1.45	1.53	0.59	0.92	0.08	0.38	0.03	0.10	0.41	0.34	3.13	0.17	0.3	0.55	0.51
		M-07	6.80	3.43	0.57	1.47	1.56	0.57	0.98	0.08	0.39	0.02	0.10	0.41	0.35	3.33	0.16	0.3	0.54	0.57
	A2	M-14	7.82	4.16	0.58	1.26	1.28	0.58	0.77	0.20	0.29	0.04	0.09	0.46	0.34	2.56	0.21	0.3	0.53	0.55
	A4	M-20	3.96	1.52	0.45	1.24	1.27	0.56	0.59	0.93	0.19	0.03	0.13	0.42	0.36	1.36	0.32	0.2	0.44	1.07
	A5	M-23	2.16	0.85	0.53	1.11	1.10	0.55	0.78	0.24	0.31	0.05	0.22	0.39	0.38	0.96	0.38	0.3	0.37	0.59
	A6	M-25	2.89	1.43	0.60	1.16	1.16	0.58	0.80	0.15	0.31	0.04	0.25	0.39	0.32	1.25	0.3	0.3	0.38	0.67
		M-27	6.10	2.96	0.55	1.35	1.33	0.56	0.82	0.24	0.25	0.03	0.11	0.40	0.33	2.75	0.2	0.3	0.55	0.38
LU	A3	M-17	7.58	5.71	1.08	1.53	1.51	0.59	0.99	0.08	0.40	0.02	0.07	0.47	0.33	2.42	0.2	0.3	0.48	0.33
		M-19	0.94	1.66	2.24	0.98	0.96	0.53	0.30	0.62	0.20	0.07	0.33	0.35	0.30	0.88	0.37	0.3	0.33	0.45

Pr: pristane, Ph: phytane, CPI: carbon preference index (2(C_{23} + C_{25} + C_{27} + C_{29})/ [C_{22} + 2(C_{24} + C_{26} + C_{28}) + C_{30}]). Ts: (C_{27} 18α(H)-22,29,30-trisnorneohopane), Tm: (C27 17α(H)-22,29,30-trisnorhopane), C_{29}/C_{30}: C_{29} norhopane/C_{30} hopane, MC$_{30}$/HC$_{30}$: C_{30} moretane/C_{30} hopane, H index: (C_{35}/(C_{31}-C_{35}) homohopane, G/C_{30}: Gammacerane/C_{30} hopane, diasterane/sterane ratio: C_{29} diasteranes/C_{29} regular steranes.

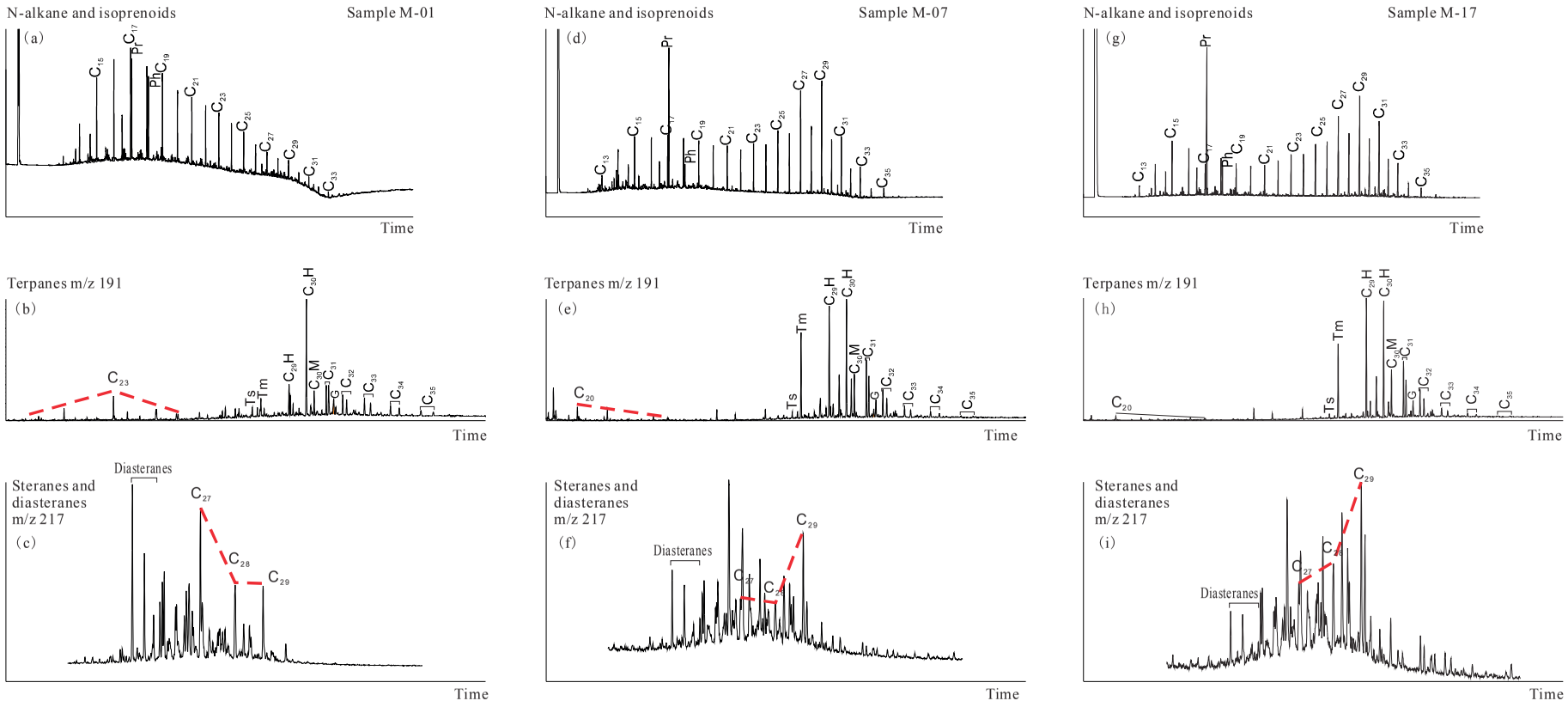

Fig. 9. (a, d, g) Gas chromatograms, (b, e, h) *m/z* 191 mass fragmentograms and (c, f, i) *m/z* 217 mass fragmentograms of saturated hydrocarbon fractions for three extracts of the Napo shales (samples M-01, M-07 and M-20).

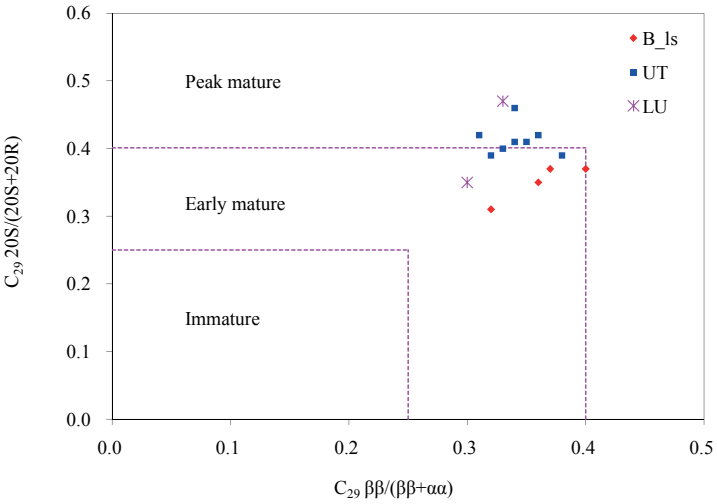

Fig. 10. Cross-plot of sterane C_{29} ββ/(ββ+αα) versus C_{29} 20S/(20S+20R), showing the level of thermal maturation of the Napo shale samples. B_ls = B limestone, UT = Upper T, U = Lower U.

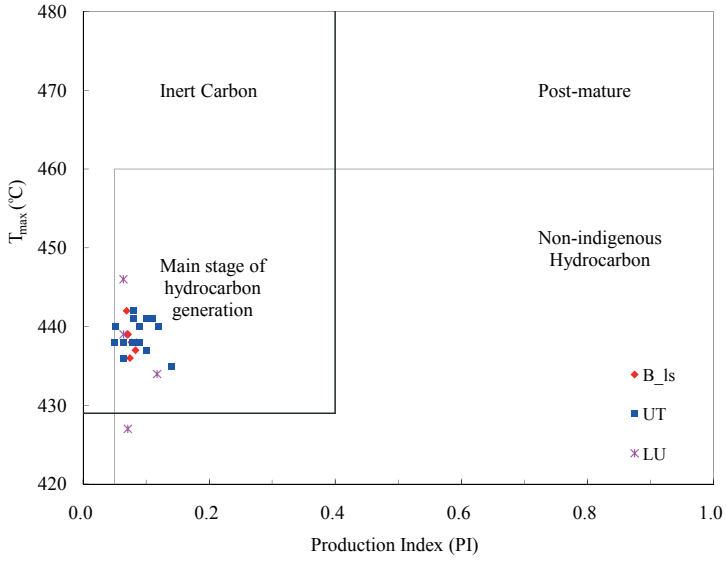

Fig. 11. Cross-plot of the production index (PI) versus T_{max}, indicating the maturity of the Napo shale samples. B_ls = B limestone, UT = Upper T, LU = Lower U.

preference (hence the low CPI and OEP values; Table 2), suggesting a significant contribution of marine, algal-derived organic matter (c.f. Brooks *et al*., 1969; Murray and Boreham, 1992; Tissot and Welte, 1984). Secondly, Fig. 9b shows a unimodal distribution with a predominance of medium to high molecular weight compounds (*n*-C_{25} to *n*-C_{31}) with minor odd-over-even carbon preference (Table 2), indicating a terrigenous organic matter input. Finally, Fig. 9c shows a bimodal distribution, suggesting a mixture of terrigenous and marine-derived organic matter.

Acyclic isoprenoids are significant in all the analysed samples (Fig. 9a, d and g). The pristane/phytane (Pr/Ph) ratio is widely used as an indicator of the redox conditions in the depositional environment and source of organic matter (Didyk *et al*., 1978; Peters *et al*., 2005; Tissot and Welte, 1984). Low Pr/Ph ratios (1.07–1.13) for the B limestone shale extracts (Table 3) suggest that these shales were deposited under suboxic-reducing conditions (Didyk *et al*., 1978; Peters *et al*., 2005; Tissot and Welte, 1984). By contrast, variable Pr/Ph (0.94–10.52) for the Lower U and Upper T shale extracts indicate terrigenous organic matter deposited under reducing-oxic conditions.

In the Lower U and Upper T intervals, the pristane concentration is always higher than *n*-C_{17} and the phytane concentration is lower than *n*-C_{18} (Table 3), resulting in high pristane/ *n*-C_{17} and low phytane/ *n*-C_{18} ratios in the range 1.43–5.71 and 0.45–0.80, respectively (Fig. 8). This indicates terrigenous organic matter deposited under suboxic conditions (Table 2).

In the B limestone interval, pristane/ *n*-C_{17} and phytane/ *n*-C_{18} ratios range from 0.90–1.16 and 1.01–1.29, respectively, further suggesting an algal marine origin and deposition under reducing conditions (Table 2; Fig. 8). The relationship between Pr/Ph and CPI (Fig. 12) is consistent with this interpretation.

These redox conditions were also indicated by the presence of pyrite associated with organic matter in the B limestone shales (Fig. 3c and d) which indicates periodically low-oxygen conditions (Hakimi *et al*., 2014; Leventhal, 1987).

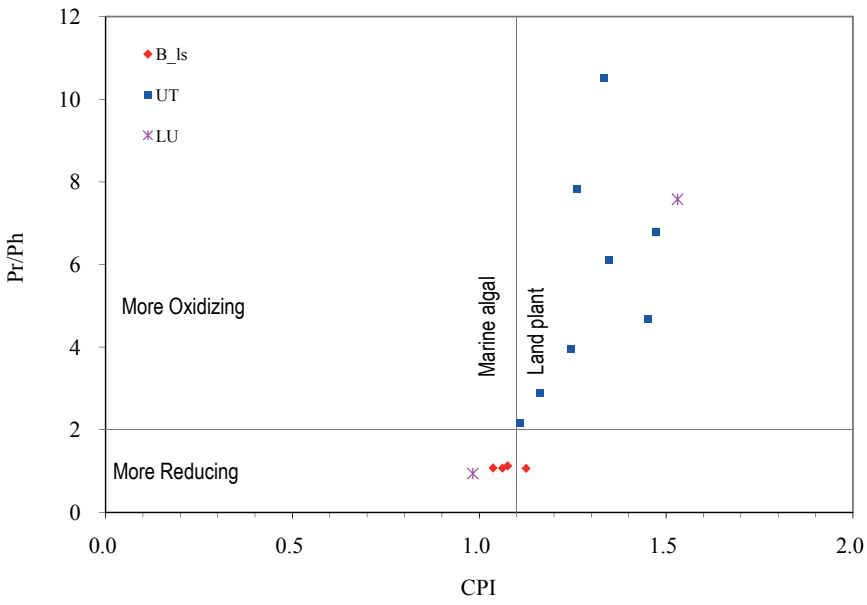

Fig. 12. Cross-plot of CPI versus pristane/phytane ratio for the the Napo shales indicating the depositional conditions (modified from Akinlua *et al.*, 2007). B_ls = B limestone, UT = Upper T, LU = Lower U.

Triterpanes and steranes

In general, the distributions of triterpanes and steranes in the Napo shale extracts can be classified into three types (Fig. 9). The analysed samples contain abundant pentacyclic triterpanes as shown by the *m/z* 191 mass fragmentograms of the saturated hydrocarbon fractions (Fig. 9b, e and h). The relative abundance of C_{29} norhopane is generally less than that of C_{30} hopane in all the studied samples (Fig. 9), with C_{29}/C_{30} 17α (H) hopane ratios in the range of 0.26 to 0.99 (Table 2). The predominance of C_{30} hopane is frequently associated with clay-rich source rocks (Gürgey, 1999). This is consistent with the lithofacies of the analysed shale extracts and is supported by high diasterane concentrations relative to regular steranes and also by mineral composition data (Fig. 9 and Table 2). Tm (C_{27} 17α(H)-22,29,30-trisnorhopane) predominates over Ts (C_{27} 18α(H)-22,29,30-trisnorneohopane), with Ts/Tm ratios ranging from 0.08 – 0.93 (Table 3). The Ts/Tm ratios are 0.61–0.92 for the B limestone samples and <0.24 for the Lower U and Upper samples.

The homohopane distributions are dominated by C_{31} homohopane and decrease with increasing carbon number (Fig. 9b, e and h). This distribution usually indicates a clastic (Waples and Machihara, 1991) or clay-rich lithofacies, as is the case of the Napo shales analysed (Obermajer *et al*., 1999). The distribution of the extended hopanes or homohopanes ($C_{31} – C_{35}$) (Fig. 9) has been used to evaluate redox conditions based on the intensity of the C_{34} and C_{35} homohopanes. Relatively high C_{34} and C_{35} homohopane concentrations are indicative of anoxic conditions in the water column during sediment deposition (Peters *et al*., 2005). In addition, gammacerane was also identified in the *m/z* 191 chromatograms of the Napo shale extracts (Fig. 9), and the gammacerane index (gammacerane/C_{30} hopane) was 0.07–0.42 (Table 3). Gammacerane index values from the B limestone samples are higher than those from the Lower U and Upper T samples. Gammacerane is a useful indicator of water column stratification during sedimentation in marine conditions and is commonly associated with hypersalinity (ten Haven *et al*., 1989; Moldowan *et al*., 1985; Peters *et al*, 2005).

The distributions of diasteranes and regular steranes (C_{27}, C_{28} and C_{29}) are illustrated by the *m/z* 217 ion chromatograms (Fig. 9, c, f, i). Relative abundances of C_{27}, C_{28} and C_{29}regular steranes were calculated and the results are given in Table 3. The distributions of C_{27}:C_{28}:C_{29} regular steranes for the B limestone samples are similar ($C_{27} > C_{28} > C_{29}$), as are the ratios of diasterane/regular sterane and the thermal maturity parameters C_{29} 20S/(20S + 20R) and the C_{29} ββ/(ββ + αα) (Table 3). The distributions of C_{27}:C_{28}:C_{29} regular steranes for the Lower U and Upper T samples are however variable ($C_{27} < C_{28} < C_{29}$, or $C_{28} < C_{29} < C_{27}$, or $C_{28} < C_{27} < C_{29}$).

A ternary plot can be used to show the relative distribution of C_{27}, C_{28} and C_{29} regular steranes (Fig. 13; Huang and Meinschein, 1979). The source input of the organic matter has a strong influence on the sterane distribution in extracts and oils, although there has been considerable debate as to the environmental significance of the distribution (Volkman, 1988). The C_{27} steranes are related to a strong algal influence, and C_{29} steranes to strong higher-plant influence (Huang and Meinschein, 1979). The analysed Napo shale samples are marine deposits. The B limestone samples display a marked dominance of C_{27} steranes, but most of the Lower U and Upper T samples show are dominated by C_{29} steranes (Table 3). The presence of C_{30} steranes (Fig. 9c, f and i) and the low C_{29}/C_{27} sterane ratio (Table 3) for the B limestone samples suggest a contribution from marine algal material to the

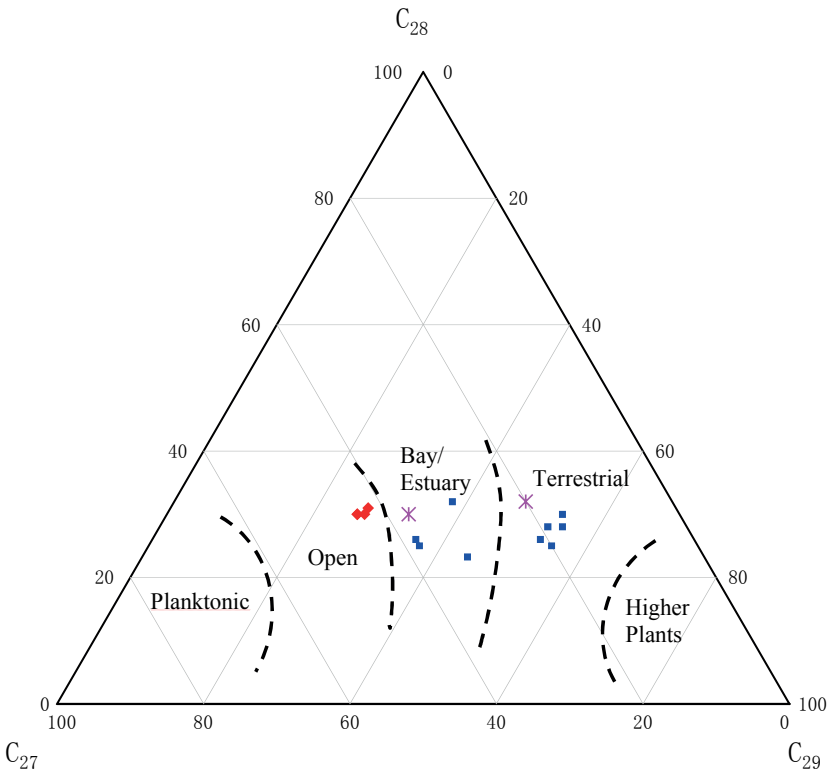

Fig. 13. Ternary diagram of regular steranes (C_{27}, C_{28} and C_{29}) showing the relationship between sterane compositions and organic matter input (modified after Huang and Meinschein, 1979). B_ls = B limestone, UT = Upper T, LU = Lower U.

source rocks, and the high C_{29}/C_{27} sterane ratio from the Lower U and Upper T samples indicates a contribution by terrigenous plants (Moldowan *et al*., 1990; Waples and Machihara, 1991). The correlation between the isoprenoids (Pr/Ph) and C_{29}/C_{27} sterane ratios for the B limestone samples (Fig. 14) also indicates a high contribution from marine algal OM deposited under reducing conditions. The relationship between Pr/Ph and gammacerane index is consistent with the inferred salinity relationship (Peters *et al.*, 2005). A cross-plot of G/C_{30} versus Pr/Ph show that most of the samples fall into the reducing and/or less oxidizing fields (Fig. 15).

In summary, the B limestone shales are interpreted to contain mostly AOM of marine algal origin deposited under anoxic and hypersaline conditions, but the coexisting AOM and SOM in the Lower U and Upper T shales is interpreted to have been derived mainly from terrigenous higher plant material with marine algal material deposited under suboxic conditions.

DISCUSSION

Canfield *et al*. (1985) proposed that the Napo Formation is in general immature in the producing area of the northern Oriente Basin, but has reached maturities sufficient for oil generation where it is buried to much greater depths in northern Peru and southern Columbia. Feininger (1975) suggested that the Cretaceous source rocks are mature to the west of the present-day Oriente Basin.

Dashwood and Abbotts (1990) reported that the Cretaceous in the Oriente Basin is generally immature to early mature, and that the Napo sediments are mature for oil generation only in the SW of the Oriente Basin and the south of the Putamayo Basin. From a reconstruction of the burial history, they estimated that the onset of oil generation for the base of the Napo Formation took place in the middle Miocene in the SW of the Oriente Basin. They suggested that the shales are immature in the eastern Oriente Basin, and that shale extracts have isotopic values which in general indicate terrigenous influenced source rocks.

However, geochemical data from oils from the Napo reservoirs showed that the source rocks for the oils were of a common facies type deposited in a predominantly marine environment. Hu *et al.* (2000) provided similar oil geochemical data, indicating that the Oriente Basin oils appear to have a strong marine affinity according to isotopic values and biomarker characteristics.

Baby *et al*. (2013) presented a map of the maturity of the Basal Napo source rock, but did not provide detailed source rock characteristics. These authors suggested that long-distance migration from the south has charged the Cretaceous reservoirs, similar to the accumulation model proposed by Dashwood and

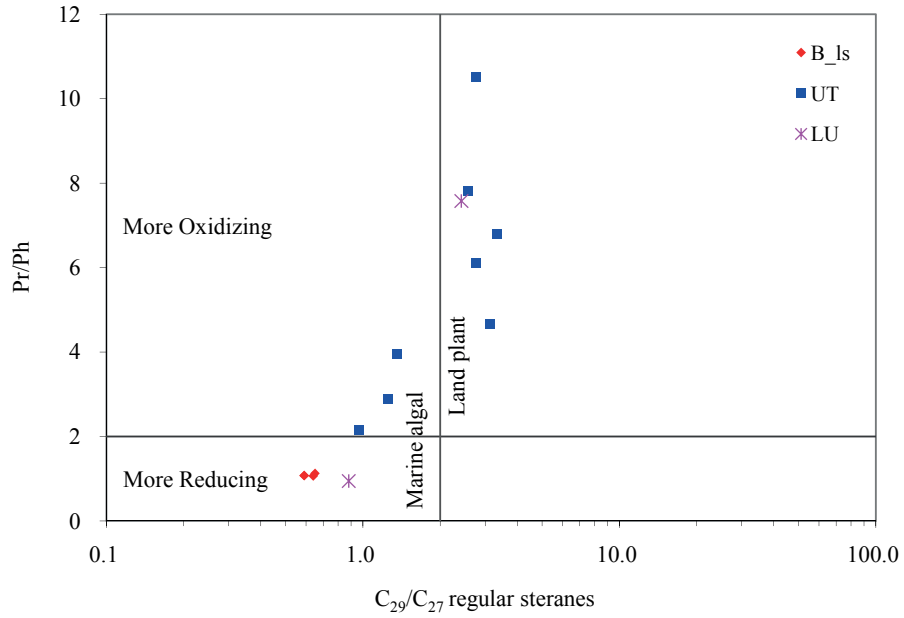

Fig. 14. Cross-plot of C_{29}/C_{27} ratio versus Pr/Ph ratio, showing the redox conditions and organic matter input. B_ls = B limestone, UT = Upper T, LU = Lower U.

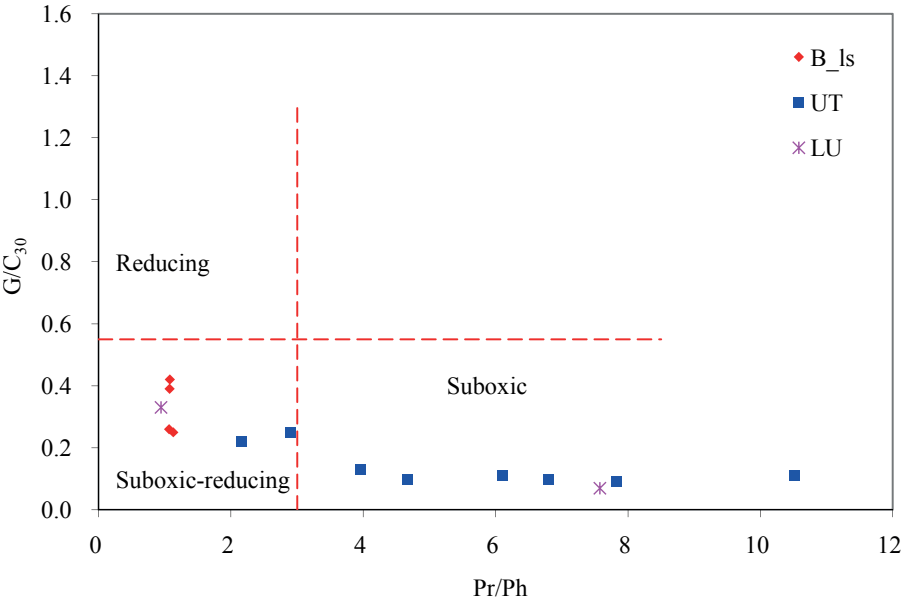

Fig. 15. Cross-plot of Pr/Ph ratio versus G/C_{30}, showing the redox conditions of the Napo shale samples. B_ls = B limestone, UT = Upper T, LU = Lower U.

Abbotts (1990) which envisaged migration distances of over 300 km from a western oil source through carrier beds in the Hollin sandstone.

Integrated with the new data presented here, however, we consider that one reason why the thermal maturity of the Napo shales, and the hydrocarbon migration processes, have not been well understood is that the presence of two types of source rock was not recognised in previous studies of the Napo Formation. The first source rock facies comprises claystone/mudstones with OM derived mainly from terrigenous higher plant material; the other consists of calcareous shales with OM of marine algal origin. This study suggests that the B limestone calcareous shales with OM of marine algal origin are a mature, effective source rock for oil generation in the eastern part of the Oriente Basin. It is likely that these calcareous shales have contributed to a significant portion of the Oriente Basin oils.

Furthermore, it should be noted that the boundaries of the individual basins within the greater Marañón-Oriente-Putumayo province are based on national frontiers, not on geological criteria. Thus the Putumayo Basin is located in Colombia, the Oriente Basin in Ecuador, and the Marañón Basin in Peru (Higley, 2001) (Fig. 1). The Oriente Basin is located in the west of the Marañón-Oriente-Putumayo province (Higley, 2001; Mathalone and Montoya, 2005) (Fig. 16a). The burial depth of the basal Napo Formation is greatest in the deepest part of the foredeep near the thrust front of the Cordillera real (Fig 16b). Here the formation is buried at depths up to about 3000 – 4000 m (9840 – 13,120 ft) based on drilling data, suggesting that it may have entered the oil window (Fig. 16b). Fig. 16b presents

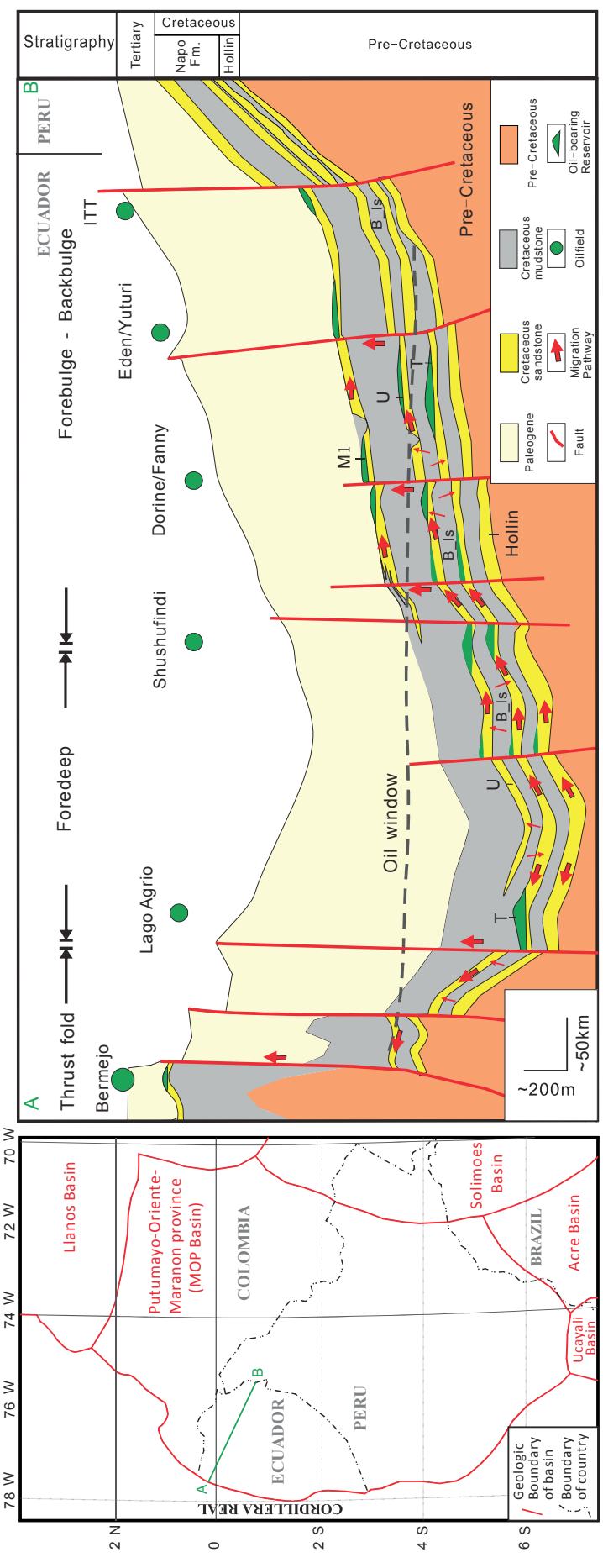

Fig. 16. General map (left) showing the location of the Oriente Basin (with boundaries which are defined by national frontiers) in the greater Marañón-Oriente-Putumayo province (which has boundaries based on geological criteria), and (right) schematic diagram showing play distribution and migration pathways for the Napo Formation in the Oriente Basin.

a schematic cross-section of the Napo Formation in the Oriente Basin showing migration pathways and potential traps.

The distribution of mature source rocks may help to explain the distribution of oil-bearing low-permeability reservoir rocks and/or stratigraphic (fluvio-deltaic or estuary sandstones) traps in the east Oriente Basin (Yang *et al*, 2016a). Future exploration of potential targets in the Napo Formation will focus not only on structural traps, but also on stratigraphic traps and low-permeability reservoir rocks adjacent to mature source rocks.

CONCLUSIONS

This study investigated organic-rich marine shales in the Lower U, B limestone, and Upper T members of the Cretaceous Napo Formation in the eastern Oriente Basin, Ecuador. Major results are as follows:

(1) The Napo shale samples analysed have TOC contents of 0.71–5.97% and hydrogen index (HI) values up to 695 mg HC/g TOC.

(2) The $\delta^{13}C$ of kerogen in shale samples from the B limestone shale ranges from -27.19 to -27.45‰, whereas the $\delta^{13}C$ values of kerogen from the Upper T and Lower U shales is > -26.30‰. Together with Rock–Eval data, this suggest that kerogen in the B limestone samples is Type II, whereas that in the Upper T and Lower U samples is mainly Type II–III with minor Type III.

(3) The B limestone shales with Type II kerogen are thermally mature, as indicated by mean vitrinite reflectance data (0.56–0.79% R_o) and Rock-Eval T_{max} (436–442 °C) as well as biomarker maturity ratios, consistent with the observation of predominantly amorphous organic matter of marine origin. By contrast, the Upper T and Lower U shales with Type II – III and III kerogens are immature to early mature, as indicated by R_o and T_{max} data (0.40–0.60% and 427–446 °C, respectively). Therefore, the B limestone shales are inferred to be an effective source rock in the east of the Oriente Basin.

(4) The saturated fraction of extracts from the B limestone shale samples is characterized by a predominance of *n*-C_{14} to *n*-C_{20} alkanes, pristane/phytane ratio ≈ 1, abundant C_{27} regular steranes and the presence of C_{30} steranes, consistent with an origin from marine algae deposited under anoxic conditions, as also indicated by the presence of abundant pyrite and of abundant amorphous organic matter. The saturated fraction of the extracts from the Lower U and Upper T shale samples contains *n*-C_{25} to *n*-C_{30} alkanes, pristane/phytane ratio > 3 and abundant C_{29} regular steranes, consistent with an origin from mainly terrigenous higher plant material mixed with marine organic matter deposited under suboxic conditions, as also indicated by the observation of coexisting amorphous and structured organic matter.

(5) This new geochemical data will contribute to an improved understanding of the distribution of low-permeability oil-bearing reservoir rocks and/or stratigraphic traps in the eastern Oriente Basin.

ACKNOWLEDGEMENTS

This work was supported by the China National Petroleum Corporation and PetroChina Company Limited (Grant No. 2014D-0906 and 2013E-0501). Additional supports were received from the National Science and Technology Major Project of China (Grant No. 2011ZX05028) and the National Science Foundation for Young Scientists of China (Grant No. 41202079). The authors are grateful to the State Key Laboratory of Petroleum Resources and Prospecting, Department of Organic Geochemistry and Environmental Science, China University of Petroleum (Beijing) for providing facilities to complete the research. The PetroChina Andes Company Ltd. kindly supplied borehole core samples of the Cretaceous in the Oriente Basin. We thank Douglas Good and Jimmy Espinosa for the assistance in the core repositories. The comments of anonymous referees on a previous version of the papeer are acknowledged with thanks.

REFERENCES

AKINLUA, A., AJAYI, T. R. and ADELEKE, B.B., 2007. Organic and Inorganic Geochemistry of Northwestern Niger Delta Oils. *Geochemical Journal*, **41**, 271-281.

BABY, P., RIVADENEIRA, M., BARRAGAN, R. and CHRISTOPHOUL, F., 2013. Thick-skinned Tectonics in the Oriente Foreland Basin of Ecuador. In: NEMCOK, M., MORA, A. and COSGROVE, J. W. (Eds), Thick-skin-dominated Orogens: From Initial inversion to Full Accretion. *Geol. Soc. Lond. Spec. Publ.*, **377**, 59-76.

BARRAGAN, R., BABY, P. and DUNCAN, R., 2005. Cretaceous Alkaline Intra-plate Magmatism in the Ecuadorian Oriente Basin: Geochemical, Geochronological and Tectonic Evidence. *Earth and Planetary Science Letters*, **236**, 670-690.

BALKWILL, H.R., RODRIGUE, G., PAREDES, F.I. and ALMEIDA, J.P., 1995. Northern Part of Oriente Basin, Ecuador: Reflection Seismic Expression of Structures. In: TANKARD, A.J., SUAREZ, S. R. and WELSINK, H.J. (Eds.), Petroleum Basins of South America. *AAPG Memoir*, **62**, 559-571.

BORDENAVE, M., 1993. Applied Petroleum Geochemistry. Editions Technip, Paris.

BROOKFIELD M.E., HEMMINGS D.P. and VAN STRAATEN P., 2009. Paleoenvironments and Origin of the Sedimentary Phosphorites of the Napo Formation (Late Cretaceous, Oriente Basin, Ecuador). *Journal of South American Earth Sciences*, **28**, 180-192.

BROOKS, J., GOULD, K. and SMITH, J., 1969. Isoprenoid Hydrocarbons in Coal and Petroleum. *Nature*, **222**, 257-259.

CANFIELD, R.W., BONILLA, G. and ROBBINS, R.K., 1985. Sacha Oil Field of Ecuadorian Oriente. *AAPG Bulletin*, **66**, 1076-1090.

CHRISTOPHOUL, F., BABY, P. and DAVILA, C., 2002. Stratigraphic Responses to a Major Tectonic Event in a

Foreland Basin: the Ecuadorian Oriente Basin from Eocene to Oligocene Times. *Tectonophysics*, **345**, 281-298.

DASHWOOD, M. F. and ABBOTTS, I. L., 1990. Aspects of the Petroleum Geology of the Oriente Basin, Ecuador. In: TANKARD, A.J., SORUCO, S.R. and WELSINK, H.J. (Eds), Classic Petroleum Provinces. *Geol. Soc. Lond., Spec. Publ.*, **50**, 89-117.

DIDYK, B.M., SIMONEIT, B.R.T., BRASSELL, S.C. and EGLINTON, G., 1978. Organic Geochemical Indicators of Palaeoenvironmental Conditions of Sedimentation. *Nature*, **272**, 216-222.

ESPITALIÉ, J., 1985. Use of T_{max} as a Maturation Index for Different Types of Organic Matter-comparison with Vitrinite Reflectance. In: Burrus, J. (Ed), Thermal Modeling in Sedimentary Basins, Editions Technip, Paris, pp. 475-496.

ESPITALIÉ, J., MADEC, M., TISSOT, J., MENNING, J. and LEPLAT, P., 1977. Source Rock Characterization Method for Petroleum Exploration. In: Offshore Technology Conference, Texas, pp. 439-448.

ESTUPIÑAN, J., MARFIL, R., DELGADO, A. and PERMANYER, A., 2007. The Impact of Carbonate Cements on the Reservoir Quality in the Napo Fm Sandstones (Cretaceous Oriente Basin, Ecuador). *Geologica Acta*, **5**, 89-107.

ESTUPIÑAN, J., MARFIL, R., SCHERER, M. and PERMANYER, A., 2010. Reservoir Sandstones of the Cretaceous Napo Formation U and T Members in the Oriente Basin, Ecuador: Links between Diagenesis and Sequence Stratigraphy. *Journal of Petroleum Geology*, **33**, 221-245.

FEININGER, T., 1975. Origin of Petroleum in the Oriente of Ecuador. *AAPG Bulletin,* **59**, 1166-1175.

GAIBOR, J., HOCHULI, J., WINKLER, W. and TORO, J., 2008. Hydrocarbon Source Potential of the Santiago Formation, Oriente Basin, SE of Ecuador. *Journal of South American Earth Sciences*, **25**, 145-156.

GÜRGEY, K., 1999. Geochemical Characteristics and Thermal Maturity of Oils from the Thrace Basin (Western Turkey) and Western Turkmenistan. *Journal of Petroleum Geology*, **22**, 167-189.

GUTSCHER, M.A., MALAVIEILLE, J., LALLEMAND, S. and COLLOT, J.Y., 1999. Tectonic Segmentation of the North Andean Margin: Impact of the Carnegie Ridge collision. *Earth and Planetary Science Letters*, **168**, 255-270.

HACKLEY, P.C. and SANFILIPO, J.R., 2016. Organic petrology and geochemistry of Eocene Suzak bituminous marl, north-central Afghanistan: Depositional environment and source rock potential. *Marine and Petroleum Geology*, **73**, 572-589.

HAKIMI, M.H., ABDULLAH, W.H., SHALABY, M.R. and ALRAMISY, G.A., 2014. Geochemistry and Organic Petrology Study of Kimmeridgian Organic-rich Shales in the Marib-Shabowah Basin, Yemen: Origin and Implication for Depositional Environments and Oil-generation Potential. *Marine and Petroleum Geology*, **50**, 185-201.

HASENHÜTTL, C., KRALJICB, M., SACHSENHOFERA, R., JELENC, B. and RIEGERA, R., 2001. Source Rocks and Hydrocarbon Generation in Slovenia (Mura Depression, Pannonian Basin). *Marine and Petroleum Geology*, **18**, 115-132.

HAVEN, H., ROHMER, M., RULLKÖTTER, J. and BISSERET, P., 1989. Tetrahymanol, the Most Likely Precursor of Gammacerane, Occurs Ubiquitously in Marine Sediments. *Geochimica et Cosmochimica Acta*, **53,** 3073-3079.

HIGLEY, D.K., 2001. The Putumayo-Oriente-Marañón Province of Colombia, Ecuador and Peru-petroleum Systems. Denver: U.S. Geological Survey.

HU, Y., YIN, J., SU, Y., XIN, Y., WANG, X., XIAO, G., YU, Z. and WANG, L., 2010. Geochemistry of Heavy Oil in the T Block, Oriente Basin and Its Origin Mechanism. *Acta Geologica Sinica*, **84**, 406-414.

HUANG, D., LI, J. and ZHANG, D., 1984. Kerogen Types and Study on Effectiveness, Limitation and Interrelation of Their Identification Parameters. *Acta Sedimentologica Sinica*, **2**, 18-33.

HUANG, W. and MEINSCHEIN, W., 1979. Sterols as Ecological Indicators. *Geochimica et Cosmochimica Acta*, **43**, 739-745.

HUNT, J.M., 1996. Petroleum Geochemistry and Geology, second ed. Freeman, New York.

JAILLARD, E., 1997. Síntesis Estratigráfica Y Sedimentológica Del Cretáceo Y Paleógeno De La Cuenca Oriental Del Ecuador. Petroproduccion, Ecuador.

HUTTON, A., BHARATI, S. and ROBL, T., 1994. Chemical and Petrographic Classification of Kerogen/Macerals. *Energy & Fuels*, **8**, 1478-1488.

JAILLARD, E., BENGTSONB, P. and DHONDT, A.V., 2005. Late Cretaceous Marine Transgressions in Ecuador and Northern Peru: A Refined Stratigraphic Framework. *Journal of South American Earth Sciences*, **19**, 307-323.

LAW, C. A. 1999. Evaluating source rocks. In: E.A. Beaumont and N.H. Foster (Eds), AAPG Special Volumes. Treatise of Petroleum Geology/Handbook of Petroleum Geology **3**, Exploring for Oil and Gas Traps, p. 6-1– 6-41. AAPG, Tulsa.

LEVENTHAL, J.S., 1987. Carbon and Sulfur Relationships in Devonian Shales from the Appalachian Basin as an Indicator of Environment of Deposition. *American Journal of Science*, **287**, 33-49.

MACKENZIE, A., PATIENCE, R., MAXWELL, J., VANDENBROUCKE, M. and DURAND, B., 1980. Molecular Parameters of Maturation in the Toarcian Shales, Paris Basin, France, i. Changes in the Configurations of Acyclic Isoprenoid Alkanes, Steranes and Triterpanes. *Geochimica et Cosmochimica Acta,* **44,** 1709-1721.

MARKSTEINER, R. and ALEMAN, A., 1997. Petroleum Systems Along the Fold Belt Associated to the Marañón-Oriente-Putumayo (MOP) Foreland Basins. VI Simposio Bolivariano Exploracion Petrolera en las Cuencas Subandinas, Memorias, Tomo ii, Asociación Colombiana de Geólogos y Geofisicos del Petróleo (ACGGP), Columbia, pp. 63-74.

MATHALONE, J.M.P. and MONTOYA, R.M., 1995. Petroleum Geology of the sub-Andean basins of Peru. In: TANKARD, A.J., SUAREZ, S. R. and WELSINK, H.J. (Eds), Petroleum Basins of South America: *AAPG Memoir*, **62**, 423-444.

MOLDOWAN, J.M., FAGO, F.J., LEE, C.Y., JACOBSON, S.R., WATT, D.S., SLOUGUI, N., JEGANATHAN, A. and YOUNG, D.C., 1990. Sedimentary 12-*n*-propylcholestanes, Molecular Fossils Diagnostic of Marine Algae. *Science*, **247**, 309-312.

MOLDOWAN, J.M., SEIFERT, W.K. and GALLEGOS, E.J., 1985. Relationship between Petroleum Composition and Depositional Environment of Petroleum Source Rocks. *AAPG Bulletin*, **69**, 1255-1268.

MUKHOPADHYAY, P., WADE, J. and KRUGE, M., 1995. Organic Facies and Maturation of Jurassic/Cretaceous Rocks, and Possible Oil-source Rock Correlation Based on Pyrolysis of Asphaltenes, Scotian Basin, Canada. *Organic Geochemistry*, **22**, 85-104.

MURRAY, A. and BOREHAM, C., 1992. Organic Geochemistry in Petroleum Exploration. Australian Geological Survey Organization, Canberra.

OBERMAJER, M., FOWLER, M. and SNOWDON, L., 1999. Depositional Environment and Oil Generation in Ordovician Source Rocks From Southwestern Ontario, Canada: Organic Geochemical and Petrological Approach. *AAPG Bulletin*, **83**, 1426-1453.

PETERS, K., 1986. Guidelines for Evaluating Petroleum Source Rock Using Programmed Pyrolysis. *AAPG Bulletin*, **70**, 318-329.

PETERS, K., WALTERS, C. and MOLDOWAN, J., 2005. The Biomarker Guide--Biomarkers and Isotopes in Petroleum Exploration and Earth History. Cambridge University Press, Cambridge, UK.

PINDELL, J. and TABBUTT, K., 1995. Mesozoic-Cenozoic Andean Paleogeography and Regional Controls on Hydrocarbon Systems. In: TANKARD, A.J., SUAREZ, S. R. and WELSINK,

H.J. (Eds.), Petroleum Basins of South America. *AAPG Memoir*, **62**, 101-128.

SHANMUGAM, G., 1985. Significance of Coniferous Rain Forests and Related Organic Matter in Generating Commercial Quantities of Oil, Gippsland Basin, Australia. *AAPG Bulletin*, **69**, 1241-1254.

SHANMUGAM, G., POFFENBERGER, M. and TORO ÁLAVA, J., 2000. Tide-dominated Estuarine Facies in the Hollin and Napo ("T" and "U") Formations (Cretaceous), Sacha Field, Oriente Basin, Ecuador. *AAPG Bulletin*, **84**, 652-682.

SMITH, L., 1989. Regional Variations in Formation Water Salinity, Hollin and Napo Formations (Cretaceous), Oriente Basin, Ecuador. *AAPG Bulletin*, **73**, 757-776.

TISSOT, B., PELET, R. and UNGERER, P., 1987. Thermal history of sedimentary basins, maturation indices, and kinetics of Oil and Gas Generation. *Geochimica et Cosmochimica Acta*, **71**, 1445-1466.

TISSOT, B. and WELTE, D., 1984. Petroleum Formation and Occurrence, Springer, New York.

TSCHOPP, H.J., 1953. Oil Explorations in the Oriente of Ecuador, 1938-1950. *AAPG Bulletin*, **37**, 2303-2347.

VALLEJO, C., HOCHULI, P., WINKLER, W. and VON SALIS, K, 2002.. Palynological and Sequence Stratigraphic Analysis of the Napo Group in the Pungarayacu 30 Well, Sub-Andean Zone, Ecuador. *Cretaceous Research*, **23**, 845-859.

VOLKMAN, J.K., 1988. Biological Marker Compounds as Indicators of the Depositional Environments of Petroleum Source Rocks. In: FLEET, A. J., KELTS, K. and TALBOT, M. R. (Eds), Lacustrine Petroleum Source Rocks. *Geol. Soc. Lond., Spec. Publ.* **40**, 103-122.

WAPLES, D. and MACHIHARA, T., 1991. Biomarkers for Geologists – a Practical Guide to the Application of Steranes and Triterpanes in Petroleum Geology. *AAPG Methods in Exploration* **9**. Tulsa, USA.

WHITE, H.J., SKOPEC, R.A., RAMIREZ, F.A., RODAS, J.A. and BONILLA, G., 1995. Reservoir Characterization of the Hollin and Napo Formations, Western Oriente Basin Ecuador. In: TANKARD, A.J., SUAREZ, S. R. and WELSINK, H.J. (Eds.), Petroleum Basins of South America. *AAPG Memoir*, **62**, 573-596.

XIE, Y., CHENG, J., SU, Y. and HU, Y., 2010. Petroleum Geology and Exploration Potential of Oriente- Marañón Basin. *Petroleum Exploration and Development*, **37**, 51-56.

YANG, X., XIE, Y., ZHANG, Z., CHEN, H., MA, Z., ZHOU, Y., WANG, D., LIU, Y., HE, Z. and ZHAO, Y., 2016a. Hydrocarbon Accumulation and Enrichment of Glauconitic Sandstone in North Oriente Basin, South America. *Chinese Journal of Geology*, **51**, 189-203.

YANG, X., XIE, Y., ZHANG, Z., MA, Z., GUO, C., ZHOU, Y., WANG, D., LIU, Y. and ZHAO, Y., 2016b. Genetic Type and Sedimentary Geological Significance of Cretaceous Glauconite in Oriente Basin, Ecuador. *Earth Science*, **41**, 1696-1708.